Spectrochimica Acta Part A: Molecular and Biomolecular Spectroscopy 209 (2019) 248–255

Contents lists available at ScienceDirect

Spectrochimica Acta Part A: Molecular and Biomolecular Spectroscopy

journal homepage: www.elsevier.com/locate/saa

Effect of intermolecular interaction on excited-state properties of thermally activated delayed fluorescence molecules in solid phase: A QM/MM study

Kai Zhang, Lei Cai, Jianzhong Fan, Yuchen Zhang, Lili Lin *, Chuan-Kui Wang *

Shandong Province Key Laboratory of Medical Physics and Image Processing Technology, School of Physics and Electronics, Shandong Normal University, 250014 Jinan, China

ARTICLE INFO

Article history:
Received 10 September 2018
Received in revised form 20 October 2018
Accepted 28 October 2018
Available online 30 October 2018

Keywords:
Thermally activated delayed fluorescence
Intermolecular interactions
Hybridized local and charge transfer state
QM/MM method

ABSTRACT

Recently, thermally activated delayed fluorescence (TADF) molecules have attracted great attention since nearly 100% exciton usage efficiency was obtained in TADF molecules. Most TADF molecules used in organic light-emitting diodes are in aggregation state, so it is necessary to make out the intermolecular interaction on their photophysical properties. In this work, the excited-state properties of the molecule AI-Cz in solid phase are theoretically studied by the combined quantum mechanics and molecular mechanics (QM/MM) method. Our results show that geometry changes between the ground state (S_0) and the first singlet excited state (S_1) are limited due to the intermolecular π-π and CH-π interactions. The energy gap between S_1 and the first triplet excited state is broadened and the transition properties of excited states are changed. Moreover, the Huang-Rhys factors and the reorganization energy between S_0 and S_1 are decreased in solid phase, because the vibration modes and rotations are hindered by intermolecular interaction. The non-radiative rate has a large decrease in solid phase which improves the light-emitting performance of the molecule. Our calculation provides a reasonable explanation for experimental measurements and highlights the effect of intermolecular interaction on excited-states properties of TADF molecules.

1. Introduction

As the third generation electroluminescent materials, thermally activated delayed fluorescence (TADF) materials have attracted great attention, and significant progress has been achieved [1–10]. >400 kinds of TADF molecular materials have been reported, while the red and blue TADF materials are still limited and new methods for designing TADF molecules are in urgent need [11–14]. In addition, most TADF molecules used in organic light emitting diodes (OLED) are prepared in film where molecules are in aggregation, and intermolecular interaction may influence the light-emitting properties of TADF molecules and also the performance of OLEDs. Aggregation-caused quenching (ACQ) phenomenon for organic light-emitting materials is often observed due to the strong intermolecular π-π interaction [15,16]. Consequently, most TADF emitters have to be dispersed into host matrices to suppress emission quenching and exciton annihilation. Nevertheless, most doped TADF-OLEDs encounter a thorny problem of swift efficiency roll-off as luminance increases [17]. Aggregation induced emission (AIE) and aggregation induced enhancement emission (AIEE) are unique photophysical phenomena offering high possibility to solve the ACQ problem [18,19]. All these phenomena indicate that intermolecular interaction has significant influence on the light-emitting properties of organic molecules, and one should always consider the intermolecular interaction in the design of organic molecules.

For TADF molecules, twisted donor–acceptor (D-A) or D-A-D configurations are the most general configurations which tend to induce loose stacking mode and weak intermolecular interaction in aggregation [20,21]. Moreover, previous investigations show that the weak intermolecular interaction produced by special molecular stacking can effectively inhibit out-of-plane vibration of the donor unit and rotation of the receptor part [22–24]. So, theoretical studies to reveal the influence of intermolecular interaction to the photophysical properties of TADF molecules are helpful for the design of TADF molecules.

In this paper, a D-A-D type TADF molecule AI-Cz (as shown in Fig. 1a) with a rigid *N*-phenylphthalimide as the acceptor unit and two carbazole groups as donor parts are studied as a model [25]. The influence of intermolecular interaction on the luminescent properties of AI-Cz is investigated using the combined quantum mechanics and molecular mechanics (QM/MM) method [26–30]. The influence mechanism will be revealed, which could help one better understand the light-emitting properties of TADF molecules in solid state and also help the design of TADF molecules.

* Corresponding authors.
E-mail addresses: linll@sdnu.edu.cn (L. Lin), ckwang@sdnu.edu.cn (C.-K. Wang).

https://doi.org/10.1016/j.saa.2018.10.053
1386-1425/

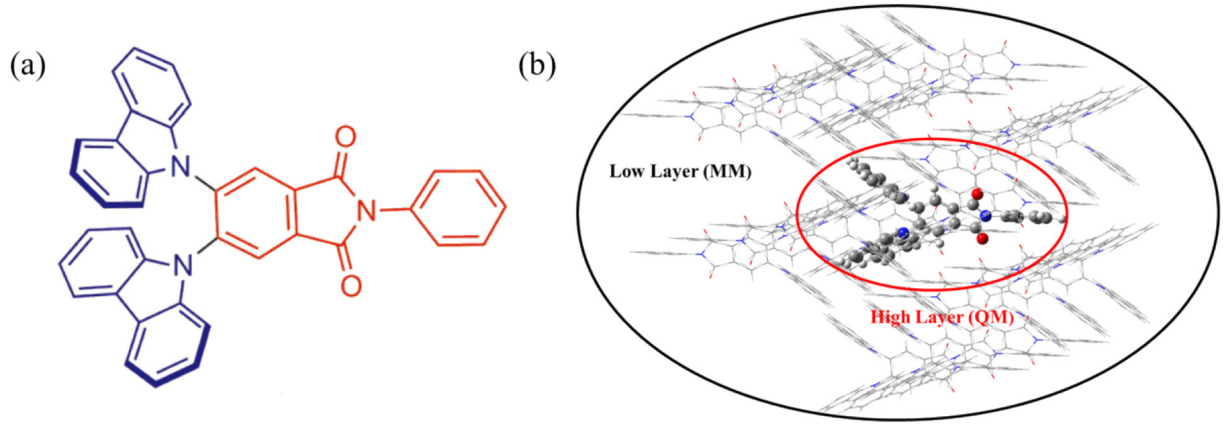

Fig. 1. (a) Geometry structure of the studied molecule AI-Cz. (b) ONIOM model: the centered molecule is treated as a high layer and the surrounding molecules are fixed as a low layer.

2. Computational Methods

Based on the crystal structure, the two layers ONIOM model is constructed (as shown in Fig. 1b) [31]. The interesting molecule is defined as a high layer and computed by QM method. The surrounding molecules are regarded as the low layer and calculated by MM method.

In order to select an appropriate functional, the absorption and emission wavelengths are calculated by different functionals including B3LYP, PBE0, BMK, CAM-B3LYP, M062X and WB97XD. Corresponding data are collected in Table 1. The absorption wavelength and emission wavelength calculated with BMK in toluene are 381 nm and 489 nm respectively, which agree with experimental values well (388 nm and 510 nm). The values calculated with BMK in solid phase are 370 nm and 525 nm, which also agree well with the experimental values (400 nm and 530 nm). Based on the absorption and emission wavelengths calculated, the optimization of geometries and excited states properties are investigated with BMK/6-31G* level, and all those calculations can be achieved in Gaussian 16 package [32]. For the calculation of ground states, the density functional theory (DFT) is adopted, while the time-dependent DFT (TD-DFT) method is used to study the properties of excited states. Moreover, the polarizable continuum model (PCM) is used to take into account the solvent effect in all simulations [33].

The photoluminescence quantum yield (PLQY) is determined by the competition between the radiative rate (k_r) and the non-radiative rate (k_{nr}). k_r is computed by the Einstein spontaneous emission rate equation which is written as

$$k_r = \frac{f\Delta E_{fi}^2}{1.499 cm^{-2}\cdot s}. \tag{1}$$

Table 1
Absorption and Emission wavelengths calculated by different functionals for studied molecule in toluene and solid phase respectively. Exp represents experimental data.

	Toluene		Solid	
	Absorption	Emission	Absorption	Emission
B3LYP	483 nm	742 nm	456 nm	594 nm
PBE0	447 nm	670 nm	426 nm	537 nm
BMK	381 nm	489 nm	370 nm	525 nm
CAM-B3LYP	380 nm	446 nm	341 nm	493 nm
M062X	356 nm	452 nm	344 nm	485 nm
WB97XD	340 nm	440 nm	333 nm	477 nm
Exp	388 nm	510 nm	400 nm	530 nm

Here f is the oscillator strength without dimension and ΔE_{fi} in units of wavenumber (cm^{-1}) is the energy difference between the initial state and the final state.

According to the Fermi's golden rule (FGR) and first-order perturbation theory, the non-radiative decay rate can be written as follows:

$$k_{nr} = \frac{2\pi}{\hbar^2}\sum_{\mu,v} P_{iv}\left|\hat{H}'_{fu,iv}\right|^2 \delta(E_{iv}-E_{fu}). \tag{2}$$

where P_{iv} is the Boltzmann distribution function of the initial state, H' is the interaction between two different Born-Oppenheimer states, and it contains two contributions as follows:

$$H\psi_{iv} = H^{BO}\Phi_i(r,Q)\Phi_v(Q) + H^{SO}\Phi_i(r,Q)\Phi_v(Q). \tag{3}$$

where H^{BO} denotes the non-adiabatic coupling and H^{SO} is the spin-orbit coupling. When the small term $\partial^2\phi/\partial Q_{fl}^2$ is neglected, the first term reads:

$$\left\langle \Phi_f\Theta_{fu}\left|H^{BO}\right|\Phi_i\Theta_{iv}\right\rangle = \sum_l \left\langle \Phi_f\Theta_{fu}\left|\left(P_{fl}\Phi_i\right)\left(P_{fl}\Theta_{iv}\right)\right|\right\rangle. \tag{4}$$

In the equation above, l is the index of the normal mode and P_{fl} is the normal mode momentum operator of the lth normal mode in the final electronic state. So the internal conversion (IC) rate constant between two electronic states with the same spin manifold can be written as:

$$k_{IC} = \frac{2\pi}{\hbar}\sum_{kl} R_{kl}Z_i^{-1}\sum_{vu} e^{-\beta E_{iv}}\langle\Phi_{fu}|P_{fk}|\Phi_{iv}\rangle\langle\Phi_{iv}|P_{fl}|\Phi_{fu}\rangle\delta(E_{iv}-E_{fu}). \tag{5}$$

Here, $R_{kl} = \langle\Phi_f|P_{fk}|\Phi_i\rangle\langle\Phi_i|P_{fl}|\Phi_f\rangle$ is the non-adiabatic electronic coupling. Further, the equation can be written as follows by applying the Fourier transform of the delta function:

$$k_{IC} = \sum_{kl}\frac{1}{\hbar^2}R_{kl}\int_{-\infty}^{\infty} dt\left[e^{i\omega_{if}t}Z_i^{-1}\rho_{IC}(t,T)\right]. \tag{6}$$

Similarly, the intersystem crossing (ISC) rate constant between two electronic states with different spin states can be written as:

$$k_{ISC} = \frac{1}{\hbar^2}\left\langle\Phi_f\left|H^{SO}\right|\Phi_i\right\rangle\int_{-\infty}^{\infty} dt\left[e^{i\omega_{if}t}Z_i^{-1}\rho_{ISC}(t,T)\right]. \tag{7}$$

Above mentioned applications can be achieved in MOMAP (Molecular Materials Property Prediction Package) program and detailed methodology can be found in Peng's and Shuai's work [34,35].

In addition, the root of the mean of squared displacement (RMSD) is adopted to characterize the geometry changes, and the formula is written as

$$RMSD = \sqrt{\frac{1}{N}\sum_{i}^{natom}\left[\left(x_i - x_i^{'}\right)^2 + \left(y_i - y_i^{'}\right)^2 + \left(z_i - z_i^{'}\right)^2\right]}. \quad (8)$$

where i is the atomic ordinal number. In order to better characterize the intermolecular interaction in the aggregation state, the δg function method of the subtraction between the initial molecular density gradient and the independent gradient model (IGM) is adopted [36]. The δg formula is written as

$$\delta g(r) = g^{IGM}(r) - g(r). \quad (9)$$

$$g(r) = \left|\sum_i \nabla\rho_i(r)\right|. \quad (10)$$

$$g^{IGM}(r) = \left|\sum_i abs[\nabla\rho_i(r)]\right|. \quad (11)$$

where i is the atomic ordinal number, $\nabla\rho(r)$ is the gradient vector, *abs* $(\nabla\rho)(r)$ represent every component of $\nabla\rho(r)$ vector takes absolute value.

3. Results and Discussions

3.1. Geometrical Structures

First, we optimized the geometry of the molecule in the ground state (S_0), the first singlet excited state (S_1), the first-triplet excited state (T_1) and the second triplet excited state (T_2) in the toluene and in solid phase respectively. Geometry changes between these states are measured by the root mean square displacement (RMSD) values which are calculated by Multiwfn, and the corresponding results are shown in Fig. 2 [37]. It can be easily seen that the geometric change between S_0 and S_1 is mainly located in the donor part in toluene (RSMD = 0.566 Å). However, the change in solid phase is obviously limited with RMSD = 0.134 Å. It indicates that geometric structures of the molecule are restrained due to the intermolecular interaction in the solid phase. Moreover, the visible comparison between S_1 and T_1, are shown in Fig. 2(b) and (e). The values of RMSD in toluene and in solid state are 0.474 Å and 0.119 Å respectively, which is slightly greater than the RMSD (0.471 Å, 0.110 Å) between S_1 and T_2 in toluene and solid phase (as shown in Fig. 2(c) and (f)). Our results indicates that molecular structure changes can be effectively hindered in solid state when the molecule transits between two states, which may induce less non-radiative energy loss of the excited state in solid state.

3.2. Energy Gaps and Transition Property

To gain deep insights into the photophysical properties in the toluene and solid phase, the frontier molecular orbitals have been examined and are plotted in Fig. 3. Results indicate that the highest occupied molecular orbitals (HOMOs) are mainly distributed in the donor unit and the lowest unoccupied molecular orbitals (LUMOs) are mainly distributed in the acceptor. The smaller overlap between HOMOs and LUMOs could result in a smaller energy gap between S_1 and T_1. The energy of the HOMO in toluene is −6.37 eV, and the energy for LUMO is −1.83 eV. The orbital energy of both HOMO and LUMO are increased in solid phase (−5.85 eV and −1.16 eV respectively). The energy gap between HOMO and LUMO is also broadened (4.69 eV in solid phase and 4.54 eV in toluene).

For TADF molecules, the energy gap between S_1 and T_1 (ΔE_{ST}) plays an important role in the RISC process. Thus, the adiabatic excitation energies for AI-Cz in toluene and solid phase are calculated respectively, and corresponding results are shown in Fig. 4. The calculated ΔE_{ST} is 0.40 eV and 0.47 eV in toluene and solid phase respectively, which indicates that intermolecular interaction could induce larger ΔE_{ST}. This is in consistence with our former results [38]. By analyzing the energy levels in toluene (Fig. 4(a)), we find that T_2 and T_3 are also below S_1 in energy, and they are close to S_1 in energy. It indicates that T_1, T_2 and T_3 may be all involved in the process of ISC and RISC processes. Furthermore, through analyzing the energy levels in the solid phase (as shown in

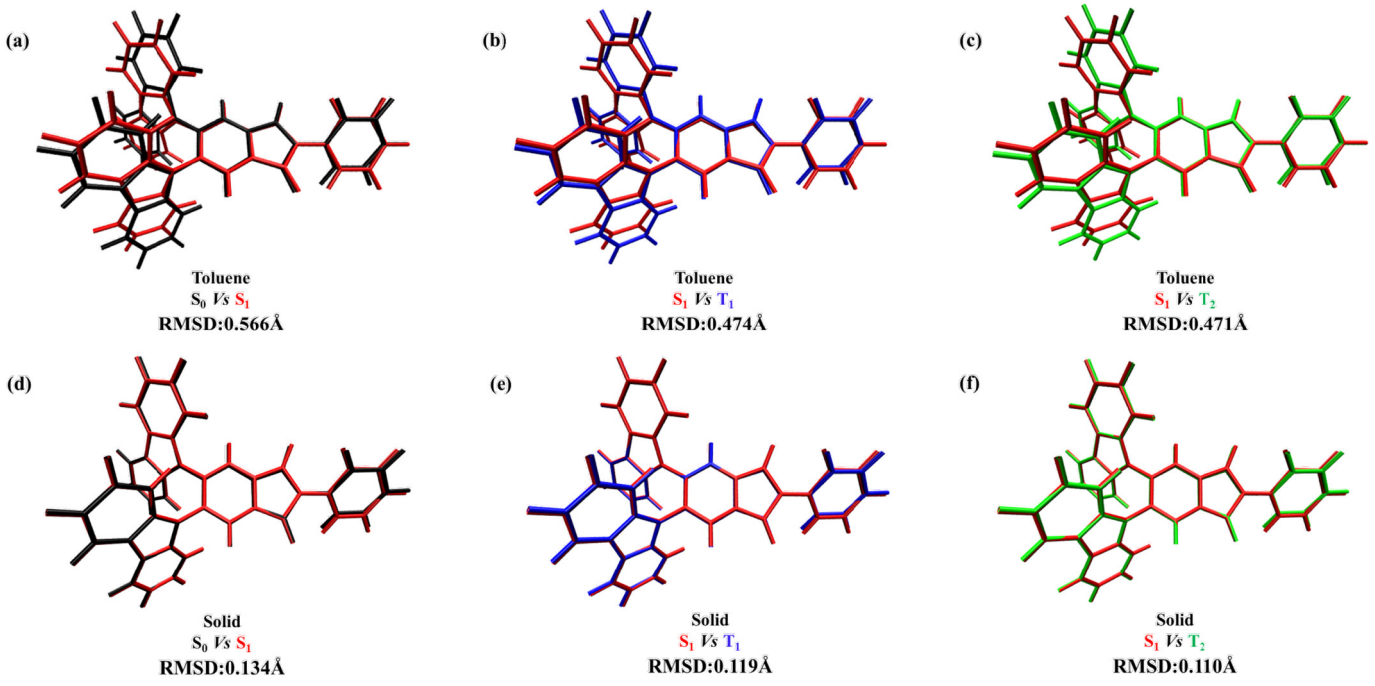

Fig. 2. Geometry comparisons between S_0 (black), S_1 (red), T_1 (blue) and T_2 (green) in toluene (a,b,c) and solid phase (d,e,f).

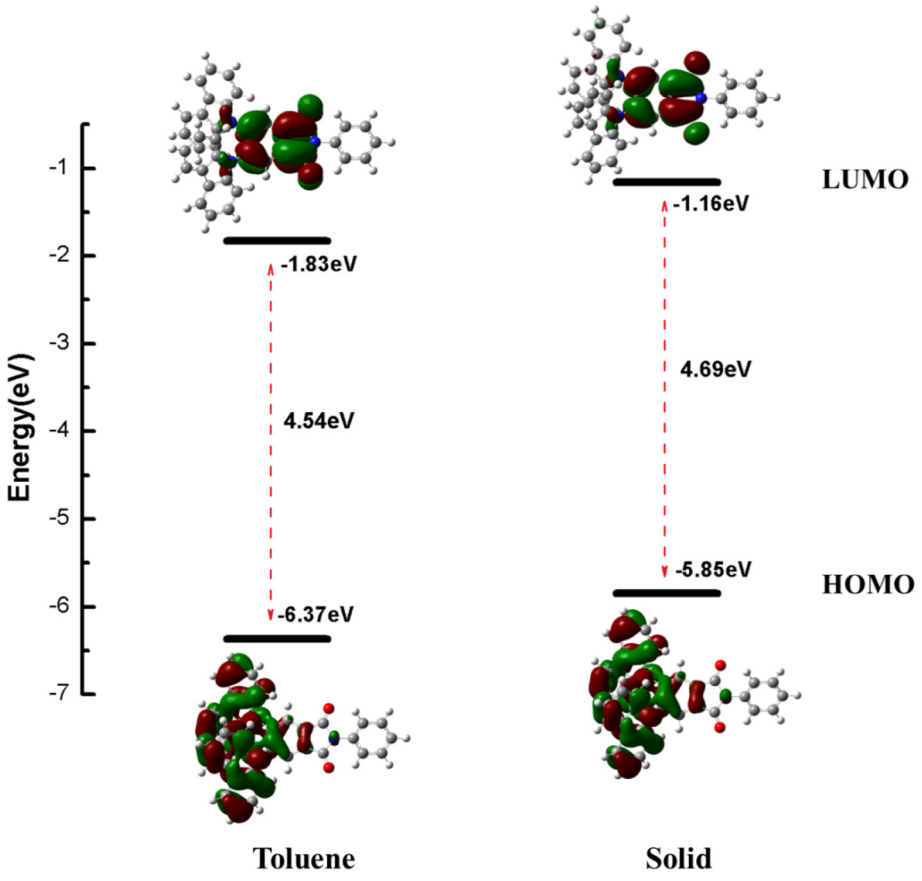

Fig. 3. Energy levels and distributions of HOMO and LUMO for molecule in toluene and solid phase (isovalue = 0.02).

Fig. 4(b)), we found that the energy of T_2 is only 0.01 eV higher than that of S_1. Therefore, in the process of ISC and RISC, T_2 may also be involved. Comparing the energy structure of the molecule in toluene and in solid phase, we conclude that intermolecular interaction in solid phase could affect the energy level structure of the molecule and also the decay channels of excited states.

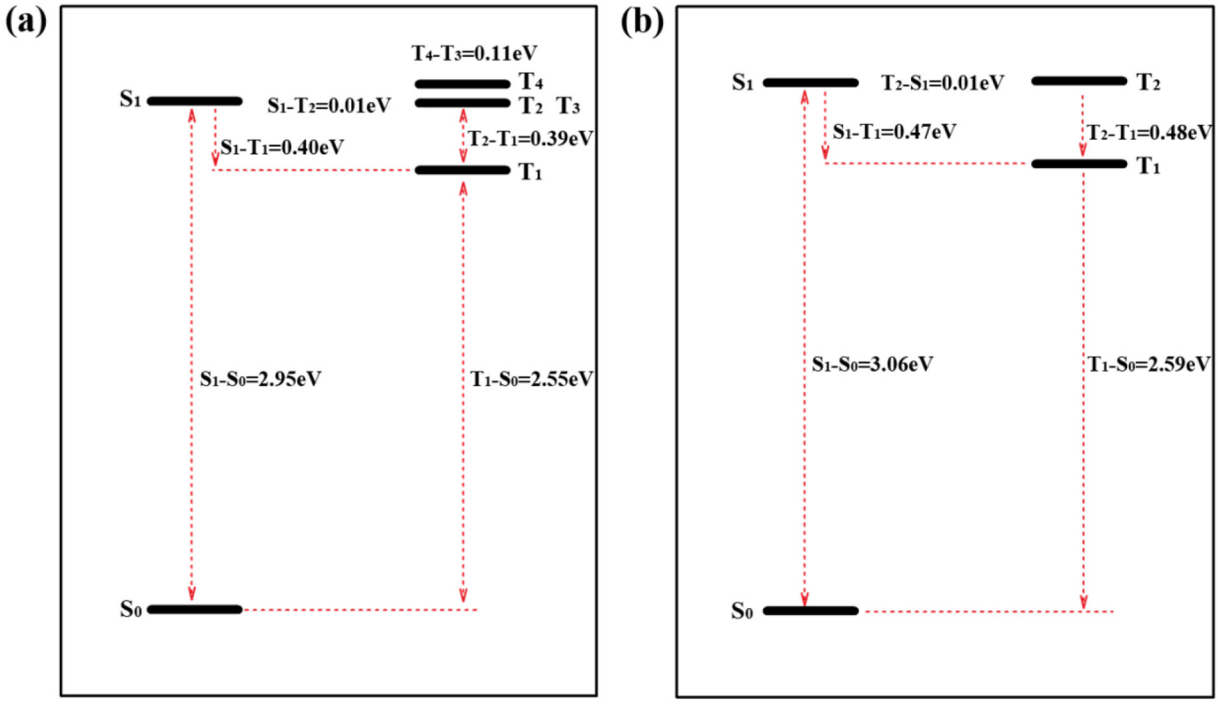

Fig. 4. Adiabatic excitation energies for AI-Cz in toluene (a) and solid phase (b) respectively.

In addition, the excited-state properties play an important role in determining the dynamics of excited states. LE, as a common state in organic light-emitting molecules, is a highly efficient radiative state, arising from its large transition moment with a larger orbital overlap [39]. The CT state, pictorialized as a pair of Coulomb bound holes and electrons, staying on the donor and acceptor parts respectively, shows a very low fluorescent efficiency, due to the forbidden electronic transition from the total spatial separation of orbitals [40]. The HLCT state is that LE and CT are highly mixed (or hybridized) to a new state [41]. The natural transition orbital (NTO) analyses for related states are performed, and the highest occupied natural transition orbital (HONTO) and the lowest unoccupied natural transition orbital (LUNTO) are calculated (shown in Fig. 5(a), and (b)). The proportion of the local-excited component in transition is also listed. Based on this value, CT (0–40%), HLCT (40–75%), and LE (75–100%) characters of both singlet and triplet excited states can be quantitatively classified [42]. We can easily find that S_1 is a charge-transfer (CT) state, while T_1 state is a hybrid local-excited and charge-transfer (HLCT) state in toluene. In the solid state, S_1 becomes the HLCT state and T_1 becomes a LE state. This indicates that the surrounding environment can change the transition properties of excited states. Moreover, the HLCT feature of S_1 in solid phase possesses the advantages of both CT states and LE states. Because CT states are useful for obtaining small ΔE_{ST}, while LE states usually have large oscillator strengths and high fluorescent efficiency [43]. Nevertheless, we find that the HLCT character of S_1 in solid state did not induce smaller ΔE_{ST} (0.47 eV in solid phase and 0.4 eV in toluene). This is due to the transition property change of T_1 which changed from HLCT to LE. Previous investigations show that triplet CT states (^{3}CT) can result in a small energy gap between singlet CT state (^{1}CT) and ^{3}CT, while triplet LE states (^{3}LE) often brings a stable triplet state and a large spin-orbit coupling (SOC) constant [44]. The larger CT component in T_1 in toluene helps the decrease of the energy gap. Although both T_2 and T_3 in toluene and T_2 in solid phase are HLCT states, the LE component has large discrepancy. For T_2 and T_3 in toluene, the LE component is about 45%, while it is about 70% for T_2 in solid phase. It may influence the spin orbit coupling between S_1 and T_2 (or T_3) [45].

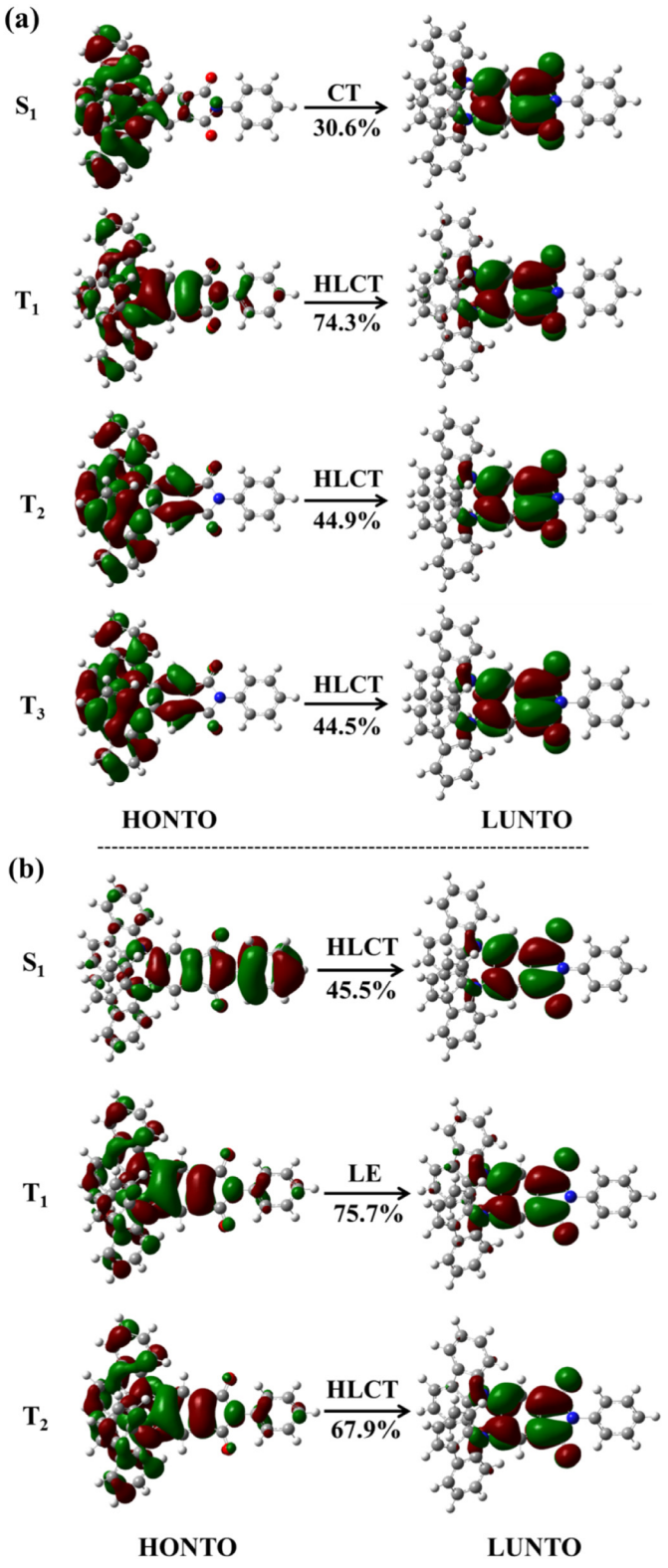

Fig. 5. Transition characteristics for singlet and triplet sates of AI-Cz in toluene (a) and solid phase (b) respectively (isovalue = 0.02). The value below every arrow represents the component of localized excitation in the corresponding transition.

Table 2
Calculated spin orbit coupling constants (cm^{-1}) between selected singlet and triplet excited states for AI-Cz in toluene and solid phase, based on their optimized structures.

Geometry	Toluene			Solid	
	$S_1\|\hat{H}_{so}\|T_1$	$S_1\|\hat{H}_{so}\|T_2$	$S_1\|\hat{H}_{so}\|T_3$	$S_1\|\hat{H}_{so}\|T_1$	$S_1\|\hat{H}_{so}\|T_2$
S_1	0.270	0.185	0.130	0.200	0.136
T_1	0.270	–	–	0.213	–
T_2	–	0.312	–	–	0.405
T_3	–	–	0.064	–	–

3.3. Excited State Dynamics

Based on the energy levels of excited states, the excited state dynamics of several excited states for AI-Cz is investigated. The spin-orbit coupling (SOC) constants (with the unit of cm^{-1}) between related singlet and triplet states calculated both in

Table 3
Calculated radiative and non-radiative rates (s^{-1}) from S_1 to S_0 as well as the ISC and RISC rates (s^{-1}) between singlet and triplet excited states. The calculated total fluorescence efficiency (Φ_F) is listed.

	Toluene	Solid
$k_r(S_1 \rightarrow S_0)$	6.30×10^6	7.98×10^5
$k_{IC}(S_1 \rightarrow S_0)$	5.20×10^{10}	1.30×10^8
$k_{ISC}(S_1 \rightarrow T_1)$	2.98×10^7	7.48×10^6
$k_{ISC}(S_1 \rightarrow T_2)$	7.30×10^5	4.48×10^5
$k_{ISC}(S_1 \rightarrow T_3)$	7.62×10^4	–
$k_{RISC}(T_1 \rightarrow S_1)$	5.77×10^0	8.82×10^{-2}
$k_{RISC}(T_2 \rightarrow S_1)$	2.01×10^6	5.95×10^6
$k_{RISC}(T_3 \rightarrow S_1)$	1.77×10^4	6.42×10^4
$k_{ISC}^{cal}(S \rightarrow T)$	2.92×10^7	7.50×10^6
$k_{RISC}^{cal}(T \rightarrow S)$	1.99×10^6	5.89×10^6
Φ_{PF}	0.01%	0.58%

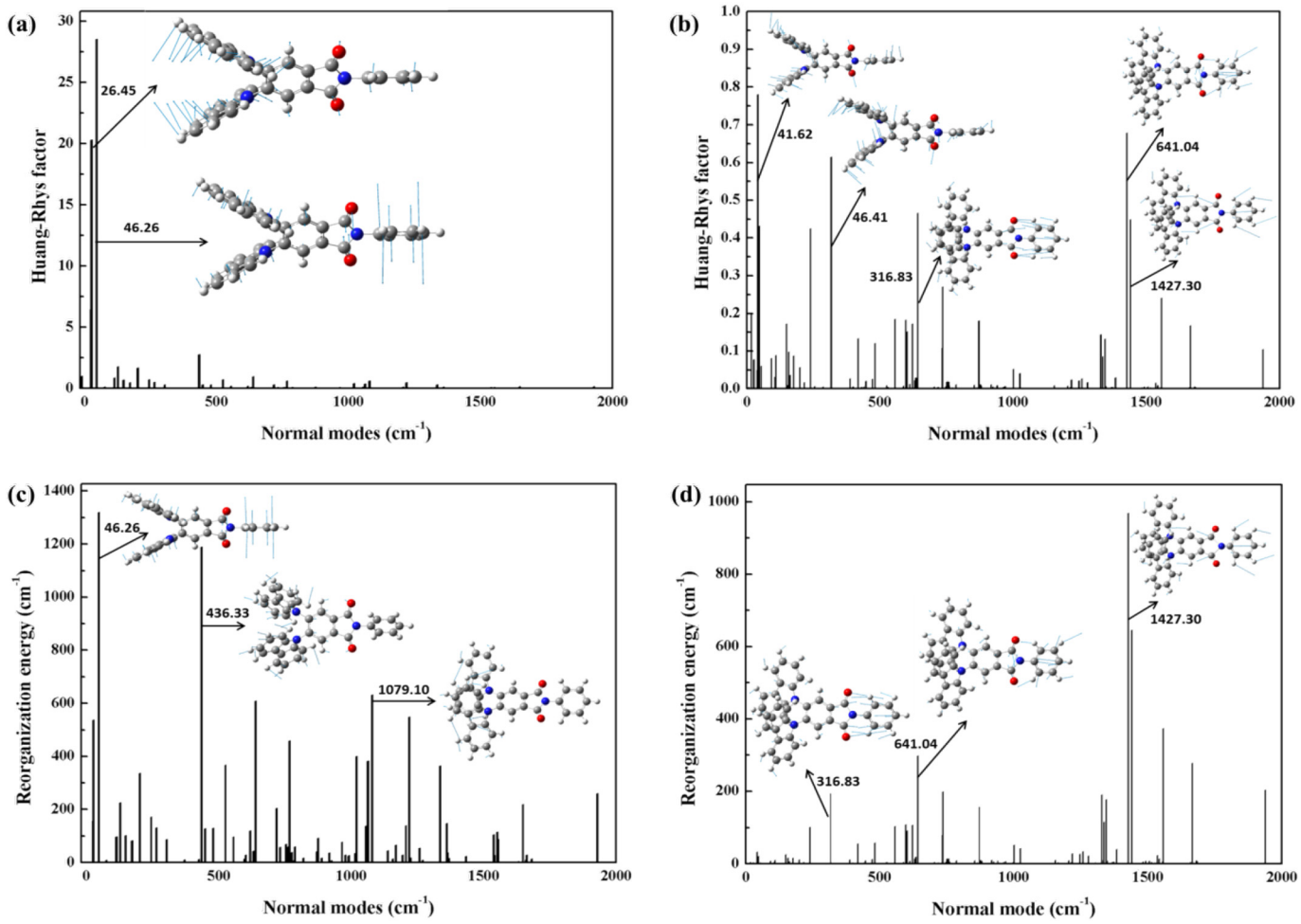

Fig. 6. Calculated HR factors versus the normal mode frequencies in toluene (a) and solid phase (b) as well as the reorganization energies versus the normal mode frequencies in toluene (c) and solid phase (d) respectively. Representative vibration modes are shown as insets.

toluene and solid phase by Dalton 2013 package are listed in Table 2 [46]. It can be found that the SOC constants between S_1 and T_1 in the liquid phase and solid phase (0.270 cm^{-1} and 0.200 cm^{-1}) calculated based on the S_1 structure have little variation comparing with the values calculated based on T_1 (0.270 cm^{-1} and 0.213 cm^{-1}). On the other hand, the SOC constants between T_2 and S_1 calculated based on T_2 structure are 0.312 cm^{-1} and 0.405 cm^{-1} in toluene and solid phase respectively, which are much larger than those calculated based on S_1 geometry (0.185 cm^{-1} and 0.136 cm^{-1}). In addition, the SOC constants between T_2 and S_1 calculated based on T_2 are also much larger than the SOC between T_1 and S_1. The SOC between T_2 and S_1 in solid state is also larger than that calculated in toluene, which may be induced by the enhancement of the LE component in T_2.

The k_r, k_{IC}, k_{ISC} and k_{RISC} between S_1 and triplet excited states are calculated (as shown in Table 3). Owing to the quasi-degenerate triplet excited states and intermediate energy levels between S_1 and T_1, we define the effective ISC and RISC rates as

$$k_{ISC}^{cal} = \frac{k_{S_1-T_1}^2 + k_{S_1-T_2}^2 + k_{S_1-T_3}^2}{k_{S_1-T_1} + k_{S_1-T_2} + k_{S_1-T_3}}. \quad (12)$$

Table 4
Reorganization energies (meV) from the bond length, bond angle, and dihedral angle in toluene and solid phase are listed respectively. $\Delta_{Toluene\text{-}Solid}$ represents the energy difference between toluene and solid phase.

	Toluene	Solid	$\Delta_{Toluene\text{-}Solid}$
Bond length	229.1	167.8	61.3
Bond angle	28.9	127.9	−99.0
Dihedral angle	171.9	48.4	123.5
Total	429.9	344.1	85.8

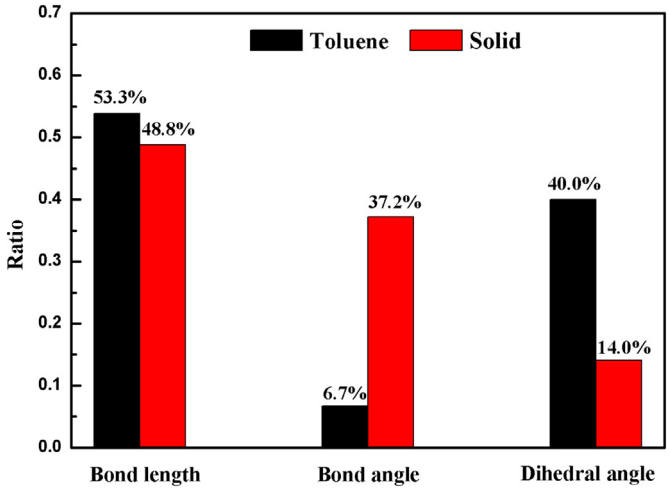

Fig. 7. Contribution ratios to the reorganization energy from bond lengths, bond angles and dihedral angles of AI-Cz in toluene and solid phase respectively.

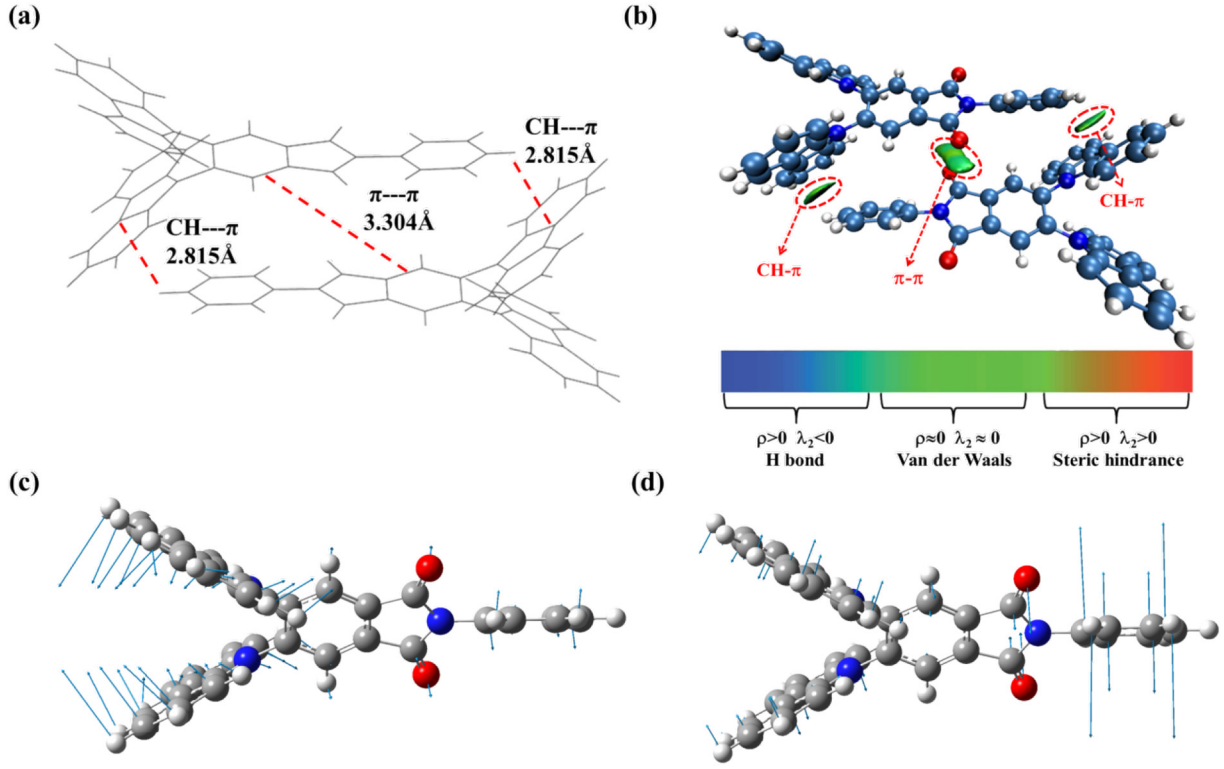

Fig. 8. (a) Intermolecular π-π and CH-π interactions. (b) Visualization of intermolecular interactions. (c) Out-of-plane vibrational of donors. (d) Rotational motion of acceptors.

$$k_{RISC}^{cal} = \frac{k_{T_1-S_1}^2 + k_{T_2-S_1}^2 + k_{T_3-S_1}^2}{k_{T_1-S_1} + k_{T_2-S_1} + k_{T_3-S_1}}. \quad (13)$$

It can be seen that the radiative decay rate k_r is smaller in the solid phase ($1.9 \times 10^5\ S^{-1}$) than that in the liquid phase ($6.3 \times 10^6\ S^{-1}$) due to the decreased transition dipole moment for AI-Cz in solid phase (2.72 Debye) compared with that in toluene (7.32 Debye). Furthermore, the calculated IC decay rate k_{IC} in solid phase ($1.38 \times 10^8\ s^{-1}$) is about two orders of magnitude smaller than that in toluene ($5.2 \times 10^{10}\ s^{-1}$). Moreover, the calculated ISC rate in solid phase ($7.48 \times 10^6\ s^{-1}$) is smaller than that in toluene ($2.98 \times 10^7\ s^{-1}$), and this is caused by the increased S_1-T_1 gap and decreased SOC constant in solid phase. Moreover, the RISC process mainly occurs from T_2 to S_1, and the transition from T_1 to S_1 can be neglected, which is caused by the large S_1-T_1 energy gap and the smaller SOC constant compared with these data between T_2 and S_1. Furthermore, the effective ISC and RISC rates are calculated to be $2.92 \times 10^7\ s^{-1}$ and $1.99 \times 10^6\ s^{-1}$ in toluene, while they are $7.5 \times 10^6\ s^{-1}$ and $5.89 \times 10^6\ s^{-1}$ in solid phase respectively. Although the effective ISC rate in solid phase is smaller than that in toluene, the RISC rate is larger. The fluorescent efficiency (Φ_{PF}) calculated in toluene is 0.01%, and it increases to 0.58% in solid phase. The luminescence efficiency is increased by >60 times in solid phase than that in toluene.

3.4. Huang-Rhys Factor and Reorganization Energy

The increase of Φ_{PF} in solid phase is mostly induced by the decreased IC rate. To make out the influence mechanism, the Huang-Rhys factor and reorganization energy close related with the IC rate are analyzed. The reorganization energy (λ) can be expressed as a sum of the contributions from normal mode analysis in the harmonic oscillator approximation

$$\lambda_{gs} = \sum_{k\in gs} \lambda_k = \sum_{k\in gs} \hbar\omega_k HR_k. \quad (14)$$

$$\lambda_{es} = \sum_{k\in es} \lambda_k = \sum_{k\in es} \hbar\omega_k HR_k. \quad (15)$$

$$HR_k = \frac{\omega_k {D_k}^2}{2\hbar}. \quad (16)$$

In the equation above, HR_k is the Huang−Rhys factor for the kth mode, and D_k represents the displacement for mode k between the equilibrium geometries of S_0 and S_1. This can be realized by the DUSHIN module in MOMAP [47]. The calculated Huang-Rhys factors versus normal modes in toluene and solid phase are shown in Fig. 6 (a) and Fig. 6(b). It can be seen that the two largest Huang-Rhys factors in toluene are larger than 20 (HR = 20.3, HR = 28.5), and corresponding vibration modes are located at 26.45 cm^{-1} and 46.26 cm^{-1} respectively. Corresponding vibration modes are mainly related to the out-plane vibration of the donors and the rotation of the acceptor. However, we easily find that the values of Huang-Rhys factor in solid phase decrease obviously and the maximum Huang-Rhys factor is <0.8. The corresponding amplitude of the out-plane vibration and the rotation is obviously reduced.

Furthermore, the reorganization energy (λ) versus vibration modes is analyzed both in toluene and solid phase, and corresponding data are shown in Fig. 6(c) and (d). We find that the reorganization energies are decreased in solid phase. Moreover, calculation results indicate that the rotational motions in low frequency regions (<500 cm^{-1}), especially for the rotation motions of donors and acceptors, are hindered in the solid phase. Meanwhile, the contribution of bond lengths, bond angles,

dihedral angles are shown in Table 4 and Fig. 7. It is found that the total reorganization energy of AI-Cz in toluene is 429.9 meV and it decreases to 344.1 meV in solid phase. The decrease in the reorganization energy (85.8 meV) in solid phase is mainly contributed by the dihedral angles (123.5 meV) which are associated with the torsional motion of donors and acceptors.

To check why the contributions to Huang-Rhys factors or reorganization energy can be effectively decreased due to the suppression of the out-plane vibration and the rotation of donors and acceptors in solid phase, the stacking structure is analyzed. Based on the X-ray structure of AI-Cz, the dimer with the closest distance is shown in Fig. 8(a). The IGM method is used to analyze the intermolecular interactions of the dimer. The visualization of interaction is shown in Fig. 8(b), and obvious green sections are found. It indicates that intermolecular π-π and CH-π interactions exist, which could effectively hinder the out-of-plane vibrational and rotational motion of donors and acceptors (as shown in Fig. 8(c) and (d)).

4. Conclusions

In this work, the influence of intermolecular interaction on the excited states properties of the TADF molecule AI-Cz have been theoretically studied in solid phase by QM/MM method. Our results indicate that intermolecular interaction could hinder the geometric change when the molecule transit between two states in solid phase. Both the energy of HOMO and LUMO as well as their gaps are increased. The energy gaps between S_1 and T_1 are also enlarged. The transition properties have also been significantly changed and the SOC values are also enhanced. Although the radiation rate is decreased in solid phase, the non-radiative rate is also significantly suppressed. By analyzing the reorganization energy, the Huang-Rhys factors and the weak intermolecular interaction in a dimer, we conclude that intermolecular interaction can effectively suppress the out-of-plane vibration mode and the rotation of donors and acceptors. Our results give good explanation of the experimental results, which could also help one better understand the influence of intermolecular interaction on the exited properties of TADF molecules.

Conflicts of Interest

There are no conflicts to declare.

Acknowledgement

This work is supported by the National Natural Science Foundation of China (Grant Nos. 11874242 and 21403133). Thanks to the supporting of Taishan Scholar Project of Shandong Province and the Scientific Research Foundation of Shandong Normal University. Thanks to the supporting of the Promotive Research Fund for Excellent Young and Middle-aged Scientists of Shandong Province (Grant No. BS2014CL001) and the General Financial Grant from the China Postdoctoral Science Foundation (Grant No. 2014M560571). Great thanks to Professor Yi Luo, Zhigang Shuai and Qian Peng for their helpful suggestions in our calculation. Thanks to Professor Yingli Niu for his great help in the usage of MOMAP.

References

[1] H. Uoyama, K. Goushi, K. Shizu, H. Nomura, C. Adachi, Nature 492 (2012) 234–238.
[2] Q. Zhang, B. Li, S. Huang, H. Nomura, H. Tanaka, C. Adachi, Nat. Photonics 8 (2014) 326–332.
[3] T. Sato, M. Uejima, K. Tanaka, H. Kaji, C. Adachi, J. Mater, Chem. C 3 (2015) 870–878.
[4] X. Xiong, F. Song, J. Wang, Y. Zhang, Y. Xue, L. Sun, N. Jiang, P. Gao, L. Tian, X. Peng, J. Am. Chem. Soc. 136 (2014) 9590–9597.
[5] M. Godumala, S. Choi, M.J. Cho, D.H. Choi, J. Mater, Chem. C 4 (2016) 11355–11381.
[6] L. Lin, Z. Wang, J. Fan, C. Wang, Org. Electron. 41 (2017) 17–25.
[7] J.-z. Fan, L.-l. Lin, C.-k. Wang, Chem. Phys. Lett. 652 (2016) 16–21.
[8] J.-z. Fan, S. Qiu, L.-l. Lin, C.-k. Wang, Chin. J. Chem. Phys. 29 (2016) 291.
[9] Q. Zhu, K. Wen, S. Feng, X. Guo, J. Zhang, Spectrochim. Acta A 192 (2018) 297–303.
[10] J. Zhang, H. Yuan, S. Feng, K. Wen, X. Guo, Spectrochim. Acta A 202 (2018) 102–106.
[11] T. Penfold, F. Dias, A. Monkman, Chem. Commun. 54 (2018) 3926–3935.
[12] M.Y. Wong, E. Zysman-Colman, Adv. Mater. 29 (2017) 1605444.
[13] T. Huang, W. Jiang, L. Duan, J. Mater. Chem. C 6 (2018) 5577.
[14] P.L. dos Santos, M.K. Etherington, A.P. Monkman, J. Mater, Chem. C 6 (2018) 4842–4853.
[15] B. Zhao, T. Zhang, B. Chu, W. Li, Z. Su, Y. Luo, R. Li, X. Yan, F. Jin, Y. Gao, Org. Electron. 17 (2015) 15–21.
[16] K. Liang, C. Zheng, K. Wang, W. Liu, Z. Guo, Y. Li, X. Zhang, Phys. Chem. Chem. Phys. 18 (2016) 26623–26629.
[17] X. Zhang, J. Zhang, J. Wang, M. Liu, Y. Xu, R. Li, Y. Chen, X.A. Li, W.-Y. Lai, W. Huang, Org. Electron. 58 (2018) 25–32.
[18] H. Tsujimoto, D.G. Ha, G. Markopoulos, H.S. Chae, M.A. Baldo, T.M. Swager, J. Am. Chem. Soc. 139 (2017) 4894–4900.
[19] J. Guo, X.L. Li, H. Nie, W. Luo, S. Gan, S. Hu, R. Hu, A. Qin, Z. Zhao, S.J. Su, Adv. Funct. Mater. 27 (2017) 1606458.
[20] V. Jankus, P. Data, D. Graves, C. Mcguinness, J. Santos, M.R. Bryce, F.B. Dias, A.P. Monkman, Adv. Funct. Mater. 24 (2015) 6178–6186.
[21] L. Yao, S. Zhang, R. Wang, W. Li, F. Shen, B. Yang, Y. Ma, Angew. Chem. 53 (2014) 2119–2123.
[22] K. Nasu, T. Nakagawa, H. Nomura, C.J. Lin, C.H. Cheng, M.R. Tseng, T. Yasuda, C. Adachi, Chem. Commun. 49 (2013) 10385–10387.
[23] L. Yu, Z. Wu, G. Xie, C. Zhong, Z. Zhu, H. Cong, D. Ma, C. Yang, Chem. Commun. 52 (2016) 11012.
[24] T. Zhang, Q. Peng, C. Quan, H. Nie, Y. Niu, Y. Xie, Z. Zhao, B.Z. Tang, Z. Shuai, Chem. Sci. 7 (2016) 5573–5580.
[25] L. Meng, L. Yanwei, D. Ruihong, W. Xiaofang, Y. Yuanping, W. Ying, C. Chuan-Feng, Angew. Chem. Int. Ed. 56 (2017) 8818–8822.
[26] J. Fan, Y. Zhang, Y. Zhou, L. Lin, C.-K. Wang, J. Phys. Chem. C 122 (2018) 2358–2366.
[27] J. Fan, L. Cai, L. Lin, C.K. Wang, Phys. Chem. Chem. Phys. 19 (2017) 29872–29879.
[28] J. Fan, L. Lin, C.K. Wang, Phys. Chem. Chem. Phys. 19 (2017) 30147–30156.
[29] L. Lin, J. Fan, C.K. Wang, Org. Electron. 51 (2017) 349–356.
[30] J. Fan, L. Cai, L. Lin, C.K. Wang, J. Phys. Chem. A 120 (2016) 9422–9430.
[31] L.W. Chung, W.M. Sameera, R. Ramozzi, A.J. Page, M. Hatanaka, G.P. Petrova, T.V. Harris, X. Li, Z. Ke, F. Liu, Chem. Rev. 115 (2015) 5678.
[32] M.J. Frisch, G.W. Trucks, H.B. Schlegel, G.E. Scuseria, M.A. Robb, J.R. Cheeseman, G. Scalmani, V. Barone, G.A. Petersson, H. Nakatsuji, X. Li, M. Caricato, A.V. Marenich, J. Bloino, B.G. Janesko, R. Gomperts, B. Mennucci, H.P. Hratchian, J.V. Ortiz, A.F. Izmaylov, J.L. Sonnenberg, Williams, F. Ding, F. Lipparini, F. Egidi, J. Goings, B. Peng, A. Petrone, T. Henderson, D. Ranasinghe, V.G. Zakrzewski, J. Gao, N. Rega, G. Zheng, W. Liang, M. Hada, M. Ehara, K. Toyota, R. Fukuda, J. Hasegawa, M. Ishida, T. Nakajima, Y. Honda, O. Kitao, H. Nakai, T. Vreven, K. Throssell, J.A. Montgomery Jr., J.E. Peralta, F. Ogliaro, M.J. Bearpark, J.J. Heyd, E.N. Brothers, K.N. Kudin, V.N. Staroverov, T.A. Keith, R. Kobayashi, J. Normand, K. Raghavachari, A.P. Rendell, J.C. Burant, S.S. Iyengar, J. Tomasi, M. Cossi, J.M. Millam, M. Klene, C. Adamo, R. Cammi, J.W. Ochterski, R.L. Martin, K. Morokuma, O. Farkas, J.B. Foresman, D.J. Fox, Gaussian 16 Rev. A.03, in, Wallingford, CT, 2016.
[33] J. Tomasi, B. Mennucci, R. Cammi, Chem. Rev. 105 (2005) 2999–3094.
[34] Z. Shuai, Q. Peng, Phys. Rep. 537 (2014) 123–156.
[35] Q. Peng, Y. Yi, Z. Shuai, J. Shao, J. Chem. Phys. 126 (2007) 1740.
[36] C. Lefebvre, G. Rubez, H. Khartabil, J.-C. Boisson, J. Contreras-García, E. Hénon, Phys. Chem. Chem. Phys. 19 (2017) 17928–17936.
[37] T. Lu, F. Chen, J. Comput. Chem. 33 (2012) 580–592.
[38] J. Fan, L. Lin, C.K. Wang, J. Mater, Chem. C 5 (2017) 8390–8399.
[39] W. Li, D. Liu, F. Shen, D. Ma, Z. Wang, T. Feng, Y. Xu, B. Yang, Y. Ma, Adv. Funct. Mater. 22 (2012) 2797–2803.
[40] A.D. Gorse, M. Pesquer, J. Phys. Chem. 99 (1995) 4039–4049.
[41] Y. Pan, W. Li, S. Zhang, L. Yao, C. Gu, H. Xu, B. Yang, Y. Ma, Adv. Opt. Mater. 2 (2014) 510–515.
[42] R. Chen, Y. Tang, Y. Wan, T. Chen, C. Zheng, Y. Qi, Y. Cheng, W. Huang, Sci. Rep. 7 (2017) 6225.
[43] W. Li, Y. Pan, L. Yao, H. Liu, S. Zhang, C. Wang, F. Shen, P. Lu, B. Yang, Y. Ma, Adv. Opt. Mater. 2 (2014) 892–901.
[44] J. Gibson, A. Monkman, T. Penfold, ChemPhysChem 17 (2016) 2956–2961.
[45] P.K. Samanta, D. Kim, V. Coropceanu, J.-L. Brédas, J. Am. Chem. Soc. 139 (2017) 4042–4051.
[46] Dalton, a molecular electronic structure program, Release Dalton2013, http://daltonprogram.org 2013.
[47] J.R. Reimers, J. Chem. Phys. 115 (2001) 9103–9109.